Forecasting synchronizability of complex networks from data

Ri-Qi Su,[1] Xuan Ni,[1] Wen-Xu Wang,[1,2] and Ying-Cheng Lai[1,3]
[1]*School of Electrical, Computer, and Energy Engineering, Arizona State University, Tempe, Arizona 85287, USA*
[2]*Department of Systems Science, School of Management and Center for Complexity Research, Beijing Normal University, Beijing 100875, China*
[3]*Department of Physics, Arizona State University, Tempe, Arizona 85287, USA*
(Received 4 January 2012; revised manuscript received 6 April 2012; published 30 May 2012)

Given a complex networked system whose topology and dynamical equations are unknown, is it possible to foresee that a certain type of collective dynamics can potentially emerge in the system, provided that only time-series measurements are available? We address this question by focusing on a commonly studied type of collective dynamics, namely, synchronization in coupled dynamical networks. We demonstrate that, using the compressive-sensing paradigm, even when the coupling strength is not uniform so that the network is effectively weighted, the full topology, the coupling weights, and the nodal dynamical equations can all be uncovered accurately. The reconstruction accuracy and data requirement are systematically analyzed, in a process that includes a validation of the reconstructed eigenvalue spectrum of the underlying coupling matrix. A master stability function (MSF), the fundamental quantity determining the network synchronizability, can then be calculated based on the reconstructed dynamical system, the accuracy of which can be assessed as well. With the coupling matrix and MSF fully uncovered, the emergence of synchronous dynamics in the network can be anticipated and controlled. To forecast the collective dynamics on complex networks is an extremely challenging problem with significant applications in many disciplines, and our work represents an initial step in this important area.

DOI: 10.1103/PhysRevE.85.056220 PACS number(s): 05.45.−a, 89.75.−k

I. INTRODUCTION

The most amazing feature of a complex dynamical system consisting of a large number of interacting units (or components) is the emergence of collective dynamics. Indeed, it is this feature of "more is different" [1] which makes complex systems extremely interesting and the study of collective dynamics fundamentally important to many natural and technological systems. Given a complex system, if the underlying mathematical rules or equations are completely known, then *in principle* the possible types of collective dynamics in the system can be predicted and studied, and most existing works on complex systems are of this nature. In realistic applications one may encounter the situation where, for a complex system of interest, the local system equations and the interactions among the components are not known *a priori* but only a set of time series are available. Can one still forecast or anticipate whether a certain type of collective dynamics can potentially occur in the system?

Even when the system equations of a complex system are known, it is still extremely challenging to predict, investigate, and explore the emergence and evolution of collective dynamics. In order to address the issue of time-series-based prediction of collective dynamics, one must focus on a relatively well known class of such dynamics. We shall then consider synchronization [2–4]. Specifically, we shall study coupled-oscillator networks [5], a paradigm for probing and understanding the synchronous behavior of interacting units with nonlinear dynamics. When the system equations are known, a widely used tool to determine whether synchronization can emerge physically is the master stability function (MSF) articulated by Pecora and Carroll [6]. In the MSF framework, synchronization under various combinations of network structures and oscillator dynamics can be predicted [5]. For example, given the nodal dynamical equations, possible states of synchronization can be determined, which are basically the possible dynamics on the synchronization manifold. The MSF is nothing but the largest Lyapunov exponent characterizing the transverse stability of the synchronous dynamical state. For a typical nonlinear or chaotic oscillator, there may exist an open interval in the space of some generalized coupling parameter [7] where the MSF is negative, so that any point in this interval can lead to stable synchronization. When the network structure is given, the set of eigenvalues of the underlying coupling matrix can be determined. For a network of coupled oscillators, the phase-space dimension can be extremely high, so there can be many transverse subspaces. The set of eigenvalues, after suitable normalization, gives the set of effective generalized coupling parameters associated with all the transverse subspaces. Network synchronization can occur only when all these parameters fall into the interval of negative MSF.

In this paper, we propose a general approach to forecasting the emergence of synchronization in complex oscillator networks based on a complete set of time series collected from all components of every oscillator. The specific setting of the problem is as follows. Assume that at the time of interest the oscillator network is in an asynchronous state and time series from each node in the network can be obtained. Assume further that there exists a parameter characterizing the average coupling strength among the nodes. The question we ask is whether it would be possible to predict that synchronization can or cannot occur when the coupling parameter is allowed to change. Our method consists of two steps. First, we reconstruct the full topology of the network, together with the coupling strengths and the nodal dynamics, based solely on time series. This is accomplished by casting the prediction or reverse-engineering [8–10] problem into the framework of compressive sensing, a recently developed, powerful convex optimization paradigm [11–15] for recovering sparse vectors based on very limited amount of data. Here the relevant vector

to be reconstructed originated from both nodal dynamics and topology, which is typically sparse due to the sparsity of complex networks. Second, from the predicted nodal dynamics and network structure, we perform synchronizability analysis by using the standard MSF approach [5]. We validate our method by using random *weighted* networks [16] of both continuous-time and discrete-time chaotic systems (e.g., the classical Lorenz system [17] and Hénon map [18]). Our computation and analysis indicate that, with only a small amount of measured data, the synchronization regions in the parameter space as identified by MSF and the network structure can be accurately predicted, rendering possible inference of synchronous dynamics. The critical data requirement and sampling frequency for different network sizes and degree distributions are studied in detail. The issue of the effect of measurement noise on prediction accuracy is also addressed. In addition, the dependence of the amount of measurements for accurate reconstruction and computational time on the network size are studied. Finally, we speculate on one potential application of our prediction method: controlling coupled oscillators to bring the system to synchronization.

In Sec. II, we describe our compressive-sensing-based method for reconstructing weighted complex oscillator networks and for estimating the MSF. In Sec. III, we present a detailed account of representative examples, together with a systematic analysis of the prediction accuracy, data requirement from different perspectives, effects of network size and noise, and computation time. In Sec. IV, we discuss how possible emergence of synchronous dynamics can be anticipated based on data. In Sec. V, a conclusion and discussion are provided.

II. NETWORK SYSTEM RECONSTRUCTION AND SYNCHRONIZABILITY ANALYSIS

A. Reverse engineering of weighted complex networked dynamical systems

Our method is in fact a combination of two schemes: compressive-sensing-based reverse engineering of complex networked dynamical systems [19,20] and synchronizability analysis [5]. Reverse engineering of complex networks to uncover network topologies from experimental time series is a problem of tremendous interest with significant applications [21–32]. Earlier examples include reconstruction of gene regulation networks [22] from gene expression data and identification of neuronal interactions based on spike classification methods [23–25]. More recently, a number of methods for network reconstruction have been proposed; these include reverse engineering of coupled differential equations [26], a response-dynamics-based method for coupled phase oscillators [27], phase-space reconstruction based on optimization [28], use of a noise-induced scaling law [29], use of a noise-induced dynamical correlation [30], random phase resetting [31], and inner composition alignment [32]. While these methods can successfully determine the network structure, they are unable to determine two pieces of key information needed for predicting the emergence of synchronization: the interaction strength among nodes and the nodal dynamical equations. As will be explained, our compressive-sensing-based method [11–15] can uncover not only the full topology of the underlying network but also the detailed nodal dynamics and link weights (interaction strengths), making it possible to forecast synchronization.

The problem of compressive sensing [11–15] can be formulated as reconstructing a sparse vector $\mathbf{X} \in \mathbb{R}^U$ with U unknown coefficients from measurement vector $\mathbf{Y}$ of M linearly independent measurements under the projection matrix $\mathbf{A}$ in the form $\mathbf{Y} = \mathbf{A} \cdot \mathbf{X}$, where $\mathbf{Y} \in \mathbb{R}^M$ and $\mathbf{A}$ is an $M \times U$ matrix. Because of the sparsity of the vector $\mathbf{X}$, the number of required measurements can usually be much smaller than the number of unknowns, i.e., $M \ll U$. Accurate reconstruction can be achieved by solving the convex optimization problem:

$$\min \|\mathbf{X}\|_1, \text{s.t. } \mathbf{A} \cdot \mathbf{X} = \mathbf{Y}. \tag{1}$$

Recently, we developed a method based on compressive sensing to infer the full network topology but for cases where the network is unweighted [20]. Here we shall show that a compressive-sensing-based framework can be formulated even for weighted complex networks, for both continuous-time and discrete-time nodal dynamics.

We first discuss the continuous-time case where the dynamics of a single isolated node is governed by

$$\dot{\mathbf{x}} = \mathbf{F}(\mathbf{x}), \tag{2}$$

where $\mathbf{x}$ is a d-dimensional vector, and $\mathbf{F}(\mathbf{x})$ is the velocity field of dimension d. Without loss of generality, we choose the parameters such that the individual nodal dynamical system generates a chaotic attractor. For a weighted network of N coupled oscillators, the system equations are

$$\dot{\mathbf{x}}_i = \mathbf{F}(\mathbf{x}_i) - \sum_{j=1}^{N} G_{ij}\mathbf{H}(\mathbf{x}_j), \quad i = 1, \ldots, N, \tag{3}$$

where $\mathbf{H}(\mathbf{x})$ is the coupling function from $\mathbb{R}^d$ to $\mathbb{R}^d$, and $\mathbf{G}$ is the $N \times N$ coupling matrix with symmetric weights $G_{ij} = G_{ji}$ and diagonal elements satisfying $G_{ii} = -\sum_{j \neq i} G_{ij}$. A nonzero G_{ij} is the necessary condition for nodes i and j to be connected, regardless of the form of the coupling function $\mathbf{H}(\mathbf{x})$.

To separate different variables we rewrite Eq. (3) in the following form:

$$\dot{\mathbf{x}}_i = \Gamma_i(\mathbf{x}_i) - \sum_{j \neq i} G_{ij}\mathbf{H}(\mathbf{x}_j), \tag{4}$$

where $\Gamma_i(\mathbf{x}_i) \equiv \mathbf{F}(\mathbf{x}_i) - G_{ii}\mathbf{H}(\mathbf{x}_i)$ is the term associated with components at node i only, which, in general, can be approximated by a power series of the d components in $\mathbf{x}_i$ up to order n in the following form:

$$[\Gamma_i]_k = \sum_{l_1=0}^{n} \cdots \sum_{l_d=0}^{n} [(a_i)_k]_{l_1,\ldots,l_d} [(\mathbf{x}_i)_1]^{l_1} \cdots [(\mathbf{x}_i)_d]^{l_d}, \tag{5}$$

for all components $k = 1, \ldots, d$. Here $[(a_i)_k]_{l_1,\ldots,l_d}$ is the coefficient assigned to each polynomial term for the kth component of node i. For many well-studied nonlinear dynamical systems, most of these coefficients are in fact zero so that the vector of coefficients is typically sparse, justifying the applicability of the compressive-sensing paradigm.

For simplicity and illustrative purpose, we choose a linear coupling form for the second term on the right-hand side of Eq. (4). Consider the simplest case where each oscillator interacts with every other oscillator through only one component. In this case, when the coupling is from the k'th component of node j to the kth component of node i, the only nonzero coupling term between nodes i and j is $[\mathbf{H}(\mathbf{x}_j)]_k = [\mathbf{x}_j]_{k'}$. A general expression for this type of linear coupling is

$$[\mathbf{H}(\mathbf{x}_j)]_h = \delta_{kh} \sum_{h'=1}^{d} \delta_{k'h'} [\mathbf{x}_j]_{h'}, \quad h = 1, \ldots, d, \tag{6}$$

where δ_{kh} is the Kronecker delta. For nonlinear coupling between multiple variables, we can group all terms containing nonzero powers of $\mathbf{x}_i$ into $\Gamma_i(\mathbf{x}_i)$.

Once we have obtained a power series expansion of the right-hand side of Eq. (4), the next step is to estimate the velocity field $\dot{\mathbf{x}}_i$ on the left-hand side, which can be extracted directly from time series by using some typical finite-difference or interpolation methods. In this way, with all expansion coefficients as unknowns, Eq. (4) can be transformed into a set of linear equations, which can be solved by using a standard compressive-sensing algorithm. After all the expansion coefficients are determined, the nonlinear nodal dynamical equations and the coupling functions are known, uncovering the full networked dynamical system including accurate estimates of the coupling weights.

To better illustrate the steps to cast the nonlinear dynamical network equations into the compressive-sensing framework, we consider a concrete example of an N-oscillator network, where the nodal dynamics of each oscillator is three dimensional ($d = 3$, say x, y, and z). In this case, we have $\mathbf{x}_i = [x_i, y_i, z_i]^T$ for $1 \leqslant i \leqslant N$. Take component x for example. According to Eq. (5), we expand $[\Gamma_i]_x$ up to order $n = 3$:

$$\begin{aligned}[\Gamma_i(\mathbf{x}_i)]_x \equiv\ & [(a_i)_x]_{000} x_i^0 y_i^0 z_i^0 + \cdots + [(a_i)_x]_{003} x_i^0 y_i^0 z_i^3 \\ & + [(a_i)_x]_{010} x_i^0 y_i^1 z_i^0 + \cdots + [(a_i)_x]_{100} x_i^1 y_i^0 z_i^0 \\ & + \cdots + [(a_i)_x]_{333} x_i^3 y_i^3 z_i^3.\end{aligned}$$

Letting $\mathbf{b}_i \equiv ([(a_i)_x]_{000}, [(a_i)_x]_{001}, \cdots, [(a_i)_x]_{333})^T$ be the coefficient vector of $[\Gamma_i(\mathbf{x}_i)]_x$, and

$$\begin{aligned}\mathbf{B}_i(t) \equiv\ & [x_i(t)^0 y_i(t)^0 z_i(t)^0, x_i(t)^0 y_i(t)^0 z_i(t)^1, \\ & \cdots x_i(t)^3 y_i(t)^3 z_i(t)^3],\end{aligned} \tag{7}$$

we have $[\Gamma_i(\mathbf{x}_i)]_x = \mathbf{B}_i \cdot \mathbf{b}_i$. Similarly, for the coupling terms we can write

$$\sum_{j \neq i} G_{ij} \mathbf{H}(\mathbf{x}_j) = \mathbf{C}_i \cdot \mathbf{c}_i$$

and

$$\begin{aligned}\mathbf{c}_i \equiv\ & \delta_{kx} [G_{i1}\delta_{k'x}, G_{i1}\delta_{k'y}, G_{i1}\delta_{k'z}, \\ & \ldots, G_{iN}\delta_{k'x}, G_{iN}\delta_{k'y}, G_{iN}\delta_{k'z}]^T,\end{aligned}$$

where node i itself is excluded. The measurement vector for node i is denoted by

$$\mathbf{C}_i(t) \equiv [x_1(t), y_1(t), z_1(t), \ldots, x_N(t), y_N(t), z_N(t)]. \tag{8}$$

If the coupling is linear and applies to a single dynamical variable, the coefficient vector $\mathbf{c}_i$ is generally sparse. The velocity vector $\dot{\mathbf{x}}_i$ can be calculated from time series at M sample times $t_1, t_2, \ldots, t_M$. Finally, we have a set of linear equations, each in the matrix form of Eq. (4):

$$\begin{pmatrix} \dot{x}_i(t_1) \\ \dot{x}_i(t_2) \\ \vdots \\ \dot{x}_i(t_M) \end{pmatrix} = \begin{pmatrix} \mathbf{B}_i(t_1) & \mathbf{C}_i(t_1) \\ \mathbf{B}_i(t_2) & \mathbf{C}_i(t_2) \\ \vdots & \vdots \\ \mathbf{B}_i(t_M) & \mathbf{C}_i(t_M) \end{pmatrix} \cdot \begin{pmatrix} \mathbf{b}_i \\ \mathbf{c}_i \end{pmatrix}. \tag{9}$$

Note that the above linear equation [33] is only for component x of node i. For the entire oscillator network, there are Nd such linear equations that need to be solved in order to fully reconstruct the network topology and the nodal dynamics. A key advantage of the compressive-sensing framework is that it requires only relatively short time-series data to accomplish this task.

We now discuss the case where the nodal dynamics are described by discrete-time maps:

$$\mathbf{x}_i[t+1] = \mathbf{F}(\mathbf{x}_i[t]) - \sum_{j=1}^{N} G_{ij} \mathbf{H}(\mathbf{x}_j[t]), \tag{10}$$

where $\mathbf{F}(\mathbf{x}_i[t])$ is the map on node i, $\mathbf{H}(\mathbf{x}_j[t])$ is the coupling function, and G_{ij} is the coupling strength. Similar to the continuous-time case, $\mathbf{G}$ is the weighted matrix. In order to estimate the derivatives of the dynamical variables, we assume that in one measurement two successive observations of the nodal states are available: $\mathbf{x}_i[t]$ and $\mathbf{x}_i[t+1]$, for all nodes in the network. In particular, the time series at t is used to construct the power series, as in the continue-time case, and the observation at $t+1$ can then be used to construct the measurement vector on the left side of Eq. (9). The networked system of discrete-time maps can then be cast into the framework of compressive sensing:

$$\begin{pmatrix} x_i[t_1+1] \\ x_i[t_2+1] \\ \vdots \\ x_i[t_M+1] \end{pmatrix} = \begin{pmatrix} \mathbf{B}_i[t_1] & \mathbf{C}_i[t_1] \\ \mathbf{B}_i[t_2] & \mathbf{C}_i[t_2] \\ \vdots & \vdots \\ \mathbf{B}_i[t_M] & \mathbf{C}_i[t_M] \end{pmatrix} \cdot \begin{pmatrix} \mathbf{b}_i \\ \mathbf{c}_i \end{pmatrix}, \tag{11}$$

where $\mathbf{B}_i[t]$ is a function of the observation of node i at t, and $\mathbf{C}_i[t]$ relies on the observation of all other nodes coupled to i at the same time t. The isolated map and the network topology (the coupling interactions) can then be extracted separately from the coefficients in $\mathbf{b}_i$ and $\mathbf{c}_i$.

B. Stability analysis for synchronous dynamics

After the nodal dynamics and the network structure have been uncovered from the time series, we can use the MSF framework to assess the emergence of synchronous dynamics and its stability [5]. For the network system of Eq. (3), the synchronous state $\mathbf{x}_1 = \mathbf{x}_2 = \cdots = \mathbf{x}_N = \mathbf{s}$, where $d\mathbf{s}/dt = \mathbf{F}(\mathbf{s})$ is an exact solution. The time evolutions of small variations from the synchronous state, $\delta\mathbf{x}_i(t) \equiv \mathbf{x}_i(t) - \mathbf{s}(t)$,

are governed by

$$\frac{d\delta\mathbf{x}_i}{dt} = \mathbf{DF}(\mathbf{s})\cdot\delta\mathbf{x}_i - \xi\sum_{j=1}^{N} G_{ij}\mathbf{DH}(\mathbf{s})\cdot\delta\mathbf{x}_j, \qquad (12)$$

where $\mathbf{DF}(\mathbf{s})$ and $\mathbf{DH}(\mathbf{s})$ are the $d\times d$ Jacobian matrices of the corresponding vector functions evaluated at $\mathbf{s}(t)$, and ξ is a parameter characterizing the global coupling strength, which can be set to unity for convenience. We denote the eigenvalues of the coupling matrix $\mathbf{G}$ as $\mu_1,\mu_2,\ldots,\mu_N$ and the associated eigenvectors as $\mathbf{e}_1,\mathbf{e}_2,\ldots,\mathbf{e}_N$. While compressive sensing does not require network connectivity, it is meaningful to explore synchronizability only when the underlying network is a single connected component. Since the network is connected, there is only one zero eigenvalue, so the eigenvalues can be sorted as $0=\mu_1<\mu_2\leqslant\cdots\leqslant\mu_N$. We then diagonalize the coupling matrix to a block matrix form composed of all the eigenvectors: $\mathbf{Q}=[\mathbf{e}_1;\mathbf{e}_2;\cdots;\mathbf{e}_N]$. This can be used in the transformation $\delta\mathbf{x}=\mathbf{Q}\cdot\delta\mathbf{y}$ to bring Eq. (12) into the following block-diagonally decoupled form:

$$\frac{d\delta\mathbf{y}_i}{dt} = [\mathbf{DF}(\mathbf{s}) - K_i\mathbf{DH}(\mathbf{s})]\cdot\delta\mathbf{y}_i, \qquad (13)$$

where $K_i=\xi\mu_i$ $(i=2,\ldots,N)$ are the coupling strengths in the oscillator network. For each K_i value, the corresponding MSF $\Psi(K)$ is the largest Lyapunov exponent of Eq. (13) [6]. If, for all possible values of K_i, the corresponding MSFs are all negative, a small perturbation about the synchronous state will vanish exponentially so that it is stable. Since MSFs do not depend on the specific network topology but on the coupling parameters, we can first infer the parameters from one set of specific measurements and calculate the MSF for arbitrary K so that the emergence of synchronous behavior can be anticipated. This can be done even when links are added or removed, because of the MSF's independence of the network structure.

After the MSF is known, the synchronization behavior of the whole oscillator network can be assessed. For example, suppose the system is not currently in a synchronous state, but there is a region of K, $K_a<K<K_b$, in which the MSF satisfies $\psi(K)<0$. We can find a suitable positive coupling strength ξ such that $K_a<\xi\mu_2<\xi\mu_N<K_b$ so as to drive the system into synchronization. This is because, under the stretching and squeezing effect of ξ, all possible K_i's can be brought into the negative MSF region.

III. EXAMPLES

To illustrate our method to forecast synchronization, we first choose the Erdős-Rényi (ER) type of homogeneous random network consisting of identical Lorenz oscillators as an example, and then we extend our study to scale-free networks and discrete-time nodal dynamics as well. In fact, similar results have been obtained for other network topologies and different types of nodal dynamics besides the cases presented here.

The classical Lorenz system is given by $[\dot{x},\dot{y},\dot{z}]=[\sigma(y-x),x(\rho-z)-y,xy-\beta z]$, where we set $\sigma=10$, $\rho=28$, and $\beta=2$ so that the oscillator is chaotic. Time-series data are generated from 6×10^6 numerical-integration steps with maximum step size of 10^{-4}. The Hénon map system is given by $[x_{t+1},y_{t+1}]=[1-ax_t^2+y_t,bx_t]$, and we set $a=1.4$ and $b=0.3$ so that the map exhibits chaotic dynamics, for which time series of length $T_N=100$ are generated. However, the amount of measurement data used in the compressive-sensing algorithm can be much smaller. Using an adjustable sampling frequency $1/\Delta T$ (or iterative interval T_N), we obtain sparse measurement data to reconstruct the nodal dynamics, coupling pattern, and the network structure. In a typical application, some physical knowledge about the underlying complex networked system may be available. This can in fact help reduce the computational complexity and increase the efficiency and accuracy significantly. For example, in the case of Lorenz-oscillator networks, some preliminary understanding of the system can facilitate the choice of the power-expansion order in Eq. (5). To be illustrative, we apply the constraint $l_1+l_2+l_3\leqslant4$ on the powers of the components x,y,z so that the number of unknown coefficients can be reduced.

The Jacobian matrix of the Lorenz system is

$$\mathbf{DF} = \begin{pmatrix} -\sigma & \sigma & 0 \\ \rho-z & -1 & -x \\ y & x & -\beta \end{pmatrix}. \qquad (14)$$

The Jacobian matrix of the coupling function, **DH**, for one specific node component, is a 3×3 matrix with only one nonzero element at the corresponding position determined by the coupling pattern. In order to compute the MSF, we need to reconstruct the network structure, find the coupling pattern, and determine the parameters characterizing the nodal dynamics.

A. Predicting weighted networks

Figure 1 shows the results of predicting a small *weighted* Lorenz-oscillator network. There are in total 122 terms in the coefficient vector $\mathbf{a}$ for each node, in which the 1st to the 35th terms correspond to nodal dynamics vector $\mathbf{b}_i$ and the rest to the coupling vector $\mathbf{c}_i$ with other nodes. The inferred coupling strengths of node No. 1 with other nodes is shown in Fig. 1(a), where, with respect to the number of power-expansion terms with nonzero coefficient values, the predicted coupling terms with other nodes are marked in Fig. 1(b). The network structure with node degrees and link weights is shown in Fig. 1(c). We see that all existent couplings, together with their corresponding link weights, have been successfully predicted. Results of prediction of all 122 terms in $\mathbf{a}$ for all three variables x,y,z in the coupled Lorenz-oscillator network are presented in Fig. 1(a). Besides the nonzero coupling terms, other nonzero terms represent various power-series terms in the nodal dynamics in each variable. The mathematical terms of nonzero terms are marked in Fig. 1(a). For example, $10y-Cy$ is in fact a combination of a nodal function and coupling, as indicated in Eq. (4). Based on the indices of the coupling terms, we can identify that the couplings are from y to x, because of the term $\sum_{j=1}^{N}G_{ij}(y_j-y_i)$ in the equation of $\dot{x}$. Therefore, the term $-Cy$ comes from $\sum-G_{ij}y_i$, which has been merged into the nodal dynamical equation. Since all coupling terms are successfully identified, the $-Cy$ term can be separated from the combination, resulting in complete

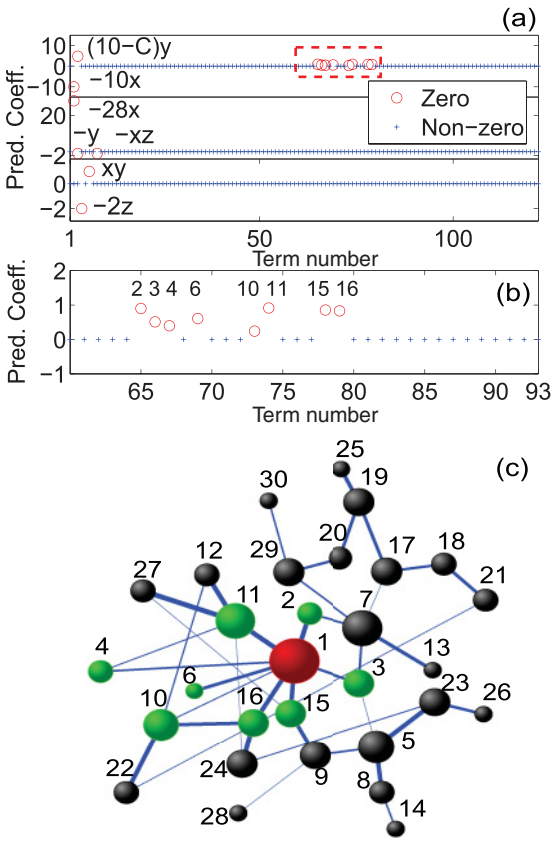

FIG. 1. (Color online) Results of detecting dynamical and coupling terms via compressive sensing. The network used is the ER random network with $N = 30$ nodes and connection probability $p = 0.04$. The network is weighted and the symmetric weights are randomly distributed in [0.1,1.0]. Panel (a) shows the prediction results for all three components x,y,z of node No. 1, where the number of data points (after sampling) used is 70% of the total number of the power-series coefficients assumed. Terms with nonzero coefficients are marked by open circles, while others are marked by plus signs. The first 35 terms are for nodal dynamical equations, and the rest are for the coupling functions. In the first panel for component x, the data points surrounded by the dashed box represent coupling-term coefficients from other node components to component x of node No. 1, which is magnified in panel (b) with numbers above data points indicating the nodes from which the couplings come. Panel (c) shows the original ER network, where the thickness of the edges indicates the corresponding coupling strength. One-to-one correspondence can be identified between the predicted coefficients in panel (b) and the coupling strengths in panel (c) for each of node No. 1's neighbors.

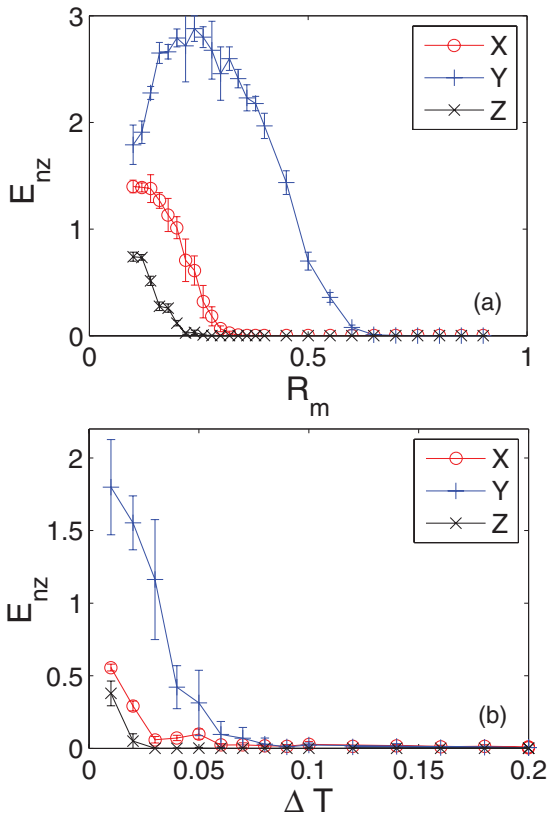

FIG. 2. (Color online) Prediction errors as functions of the normalized amount of measurement, R_m, and sampling interval ΔT for a random symmetric weighted network of $N = 60$ Lorenz oscillators, where the connection probability is $p = 0.04$ and the weights are randomly distributed in [0.1,1.0]. There are possibilities that the generated networks are disconnected, but in order to be able to consider synchronizability, we disregard rare cases where the networks generated consist of isolated components. In (a), the sampling interval is fixed at $\Delta T = 0.1$, whereas in (b), the amount of measurement is fixed at $R_m = 0.6$. In both panels, E_{nz} is averaged over 10 independent network realizations.

prediction of all power-series terms in the velocity field and the coupling function associated with node No. 1. We have also examined the prediction results for all other nodes in the network and found excellent agreement between the predicted and actual power-series terms governing the whole networked dynamical system.

The efficiency of our method for reconstructing weighted networks can be assessed by addressing the issue of data requirement and sampling frequency when nearly perfect prediction accuracy is achieved. It is useful then to define prediction errors in the coefficient vector **a**. Since **a** is sparse, i.e., most of its elements are zero, it is necessary to calculate the errors for nonzero (existing) and zero (nonexisting) terms separately. In particular, the relative error of a nonzero term, E_{term}, is defined as the ratio to the true value of the absolute difference between the inferred and the true values. The prediction error E_{nz} of all nonzero terms in a component,

$$E_{nz} \equiv \langle E_{\text{term}} \rangle,$$

is the average over them. For a zero term, a relative error cannot be defined. As an alternative, we define the absolute error as the average value of the inferred zero terms. The prediction errors can then be computed as functions of the amount R_m of measurements, normalized by the total number of unknown coefficients to be determined, i.e.,

$$R_m \equiv \frac{\text{number of measurements}}{\text{number of all unknown coefficients}},$$

and the sampling time interval ΔT, as shown in Fig. 2, where ΔT is the average time interval between two pairs of data points, with each pair containing two nearby data points for

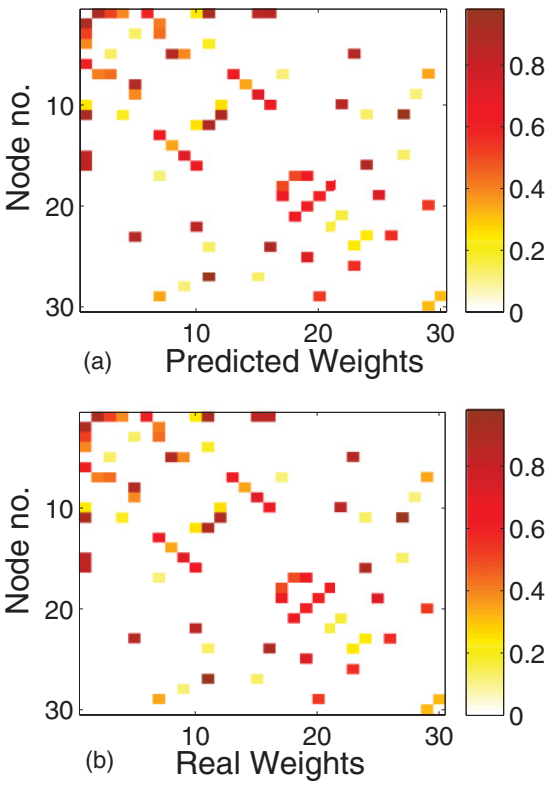

FIG. 3. (Color online) Comparison of the reconstructed (a) and the original (b) adjacency matrices for the weighted network shown in Fig. 1(c). The coupling scheme is $y \to x$ and the normalized amount of measurements is $R_m = 0.3$.

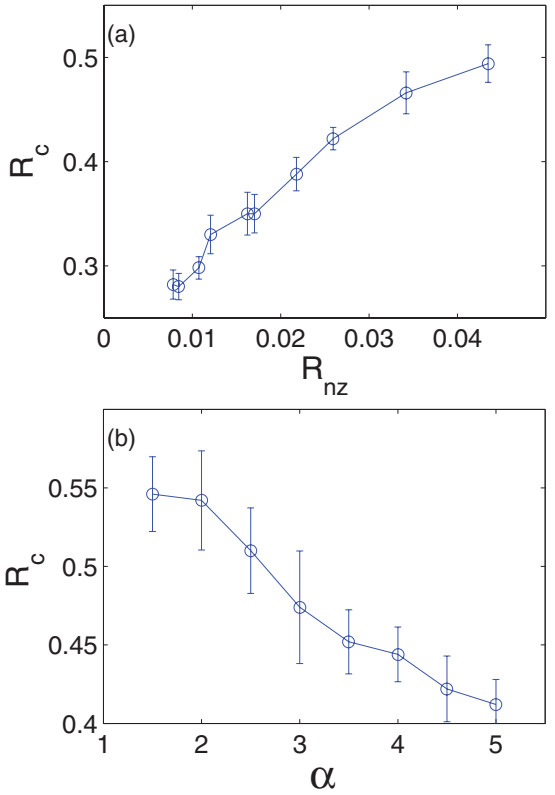

FIG. 4. (Color online) (a) For ER random networks, measure of critical data requirement R_c as a function of the density of nonzero coefficients R_{nz}, where R_{nz} is adjusted by fixing the average degree at $k = 3$ and increasing the network size from $N = 20$ to $N = 200$. (b) For scale-free networks, R_c as a function of the power-law exponent α in the degree distribution $p(k) \sim k^{-\alpha}$. The network size is $N = 60$ with the minimal degree $k_{\min} = 3$. For both panels, the data points are results of averaging over 10 different network realizations.

the purpose of estimating the corresponding derivative. In Fig. 2(a), we see that, for sufficiently large values of R_m, E_{nz} reduces essentially to zero with extremely small error bars, indicating accurate reconstruction of both nodal dynamics and network structures with complete information about the locations of the links and their weights. From Fig. 2(b), we observe that a larger sampling interval ΔT tends to facilitate prediction. This can be intuitively understood by noting that suitably large ΔT values weaken the correlation between two adjacency data points, from which reconstruction may benefit. In both Figs. 2(a) and 2(b), the Y component appears to be the most difficult one to be fully reconstructed, as the required data amount is the largest. This is due to the presence of the ρx term in the Y component, where the value of the coefficient ρ is much larger than other nodal dynamical and coupling coefficients, requiring more measurements and larger sampling intervals. Our experience indicates that, in general, the data requirement for equations that involve relatively larger coefficients tends to be higher.

In order to assess the accuracy of the predicted weighted network, it is necessary to reconstruct the adjacency matrix for any given coupling scheme. With all expansion coefficients obtained from compressive sensing for all dynamical variables of each oscillator, we can readily form the matrix by using the terms associated with the various coupling functions. For example, coupling coefficients from each node contribute to a single row of the adjacency matrix, given any coupling scheme. Figure 3 shows, for the $y \to x$ coupling scheme, the reconstructed and the original adjacency matrices. The good agreement between the two suggests that not only have the link locations been predicted but also the *values of the corresponding weights*.

To further address the practically important issue of data requirement in reconstructing weighted networks, we define a quantity R_c, which is the critical amount of data required for the prediction error E_{nz} to fall below some predefined small threshold value (e.g., 0.01), namely,

$$R_c \equiv \inf\{R_m : E_{nz}(R_m) \leqslant 0.01\}.$$

Although R_c depends on the choice of the threshold, the qualitative behavior of R_c is insensitive to the network structure. For example, we can calculate R_c for different ratios R_{nz} defined as

$$R_{nz} \equiv \frac{\text{number of nonzero coefficients}}{\text{number of all unknown coefficients}},$$

where R_{nz} can be adjusted by varying the network size while keeping the average degree unchanged. Figure 4(a) shows R_c versus R_{nz} for different ER random networks. We see that, as R_{nz} becomes smaller so that the network becomes more sparse, the value of R_c tends to decrease, indicating that a smaller amount of data is required to achieve the same prediction

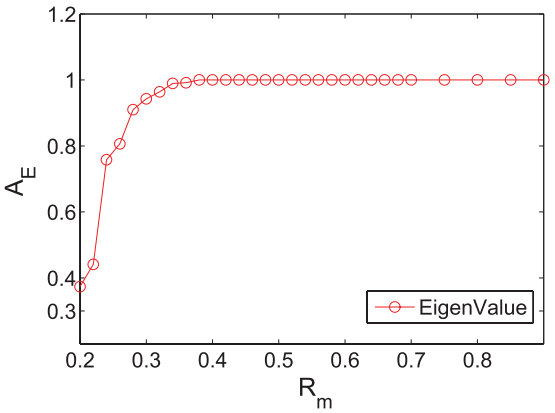

FIG. 5. (Color online) For the random Lorenz network under the coupling scheme $y \to x$, accuracy measure A_E of the eigenvalue spectrum of the reconstructed network coupling matrix as a function of the normalized data amount R_m.

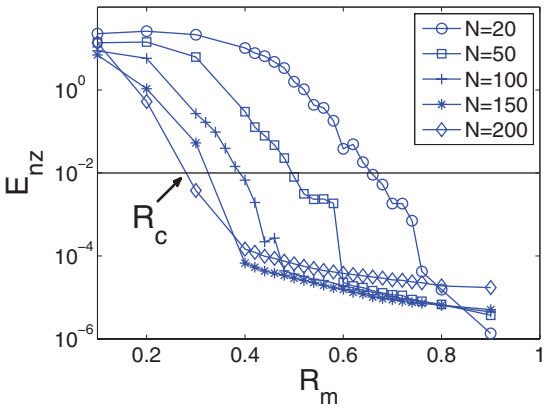

FIG. 6. (Color online) For weighted, random networks of Hénon maps, prediction errors as functions of the normalized data amount R_M. The network size varies from 20 to 200, and all the networks tested have the same connection probability $p = 0.04$ with weights distributed in $[5 \times 10^{-4}, 10^{-3}]$. Each point is the result of averaging over 10 independent network realizations. The horizontal solid line at $E_{NZ} = 0.01$ is used to indicate the critical data requirement R_C for each case.

accuracy. This is due to the merit of our compressive-sensing-based method in dealing with large networks, i.e., low data requirement. This feature does not depend on the network topology either, as shown in Fig. 4(b) for scale-free networks, where R_c is shown as a function of α, the power-law exponent in the degree distribution. When the network size and the average degree are fixed, a smaller value of α corresponds to a more heterogeneous network structure. In this case, the value of R_c is relatively large. This is because, for a more heterogeneous network, the probability of having dense sets of coefficients for the hub nodes is larger, requiring more data. As α is increased so that the network becomes less heterogeneous, R_c can be reduced.

Eigenvalues of the network coupling matrix can be calculated upon determining the structural parameters of the network. It is thus useful to define another quantity to characterize the accuracy of the reconstructed weighted network. Specifically, we first define the eigenvalue interval that contains all the original eigenvalues as $R'_t = (K_2, K_N)$ and the predicted one as $R'_p = (K'_2, K'_N)$. We then define the following quantity A_E to characterize the accuracy of the reconstructed eigenvalue spectrum:

$$A_E = \frac{R'_p \bigcap R'_t}{R'_p \bigcup R'_t} = \frac{\min(K_N, K'_N) - \max(K_2, K'_2)}{\max(K_N, K'_N) - \min(K_2, K'_2)}. \quad (15)$$

Here we use a continuous region instead of a set of individual eigenvalues of the coupling matrix for the definition of the true region R'_t, because the necessary condition for the system to be synchronizable is that all eigenvalues must be located in the negative region of MSF $\Psi(K)$. Since the MSF is not involved in the definition of A_E, a convenient choice is to compare the region from the minimum nonzero eigenvalue K_2 to the maximum K_N, which limits our discussion within the systems possessing the type of MSF [see, e.g., Fig. 9(b)]. A representative plot of A_E as a function of R_m is shown in Fig. 5. We see that the eigenvalue spectrum can be predicted accurately when R_m exceeds about 35%, due to the low data requirement of compressive sensing.

Similar results are obtained from networks of Hénon map systems. In the following examples we discuss the effect of the network size and noise on system reconstruction and also the issue of computational time. To be illustrative, we assumed weighted random networks with weights distributed in the range $w_{ij} \in [5 \times 10^{-4}, 10^{-3}]$ (so that dynamical trajectories from the Hénon map do not diverge). The coupling function is chosen to be linear, and it occurs between the x variables among the nodes. Applying the compressive sensing algorithm allows us to infer the nodal dynamics and network topology from the coefficients **a**.

The performance of our method with respect to different network size is an important issue. As shown in Fig. 6, as the data amount R_m is increased, for different network sizes ranging from $N = 20$ to $N = 200$, the normalized predicted errors E_{nz} approach zero, as indicated by the horizontal solid line, suggesting that the system can be reconstructed with high accuracy based on a small amount of data, regardless of the network size. While slightly more data are required for larger networks, the amounts are still quite small, i.e., less than the total number of unknown coefficients in the power-series expansion. We also find that the critical data ratio R_c, defined as the relative data amount required to make the normalized predicted error E_{nz} less than a small threshold value (e.g., 0.01), decreases with the network size N. This is in accordance with the results in Fig. 4(a), since the degree of sparsity of the unknown vector **a** increases with the random network size as the connection probability p is fixed.

Another issue that we have studied is the effect of measurement noise on reconstruction. In our framework, observations of the variable states in one measurement are associated with the state of the system at the particular time, so measurement noise can be quite important. Figure 7 shows the reconstruction result when additive noise of amplitude 5×10^{-5} is present. We see that compressive sensing is capable of generating approximate solutions of the networked system even in the presence of noise. The data amount required to reconstruct the network, however, tends to be slightly larger than that in the case where no noise is present.

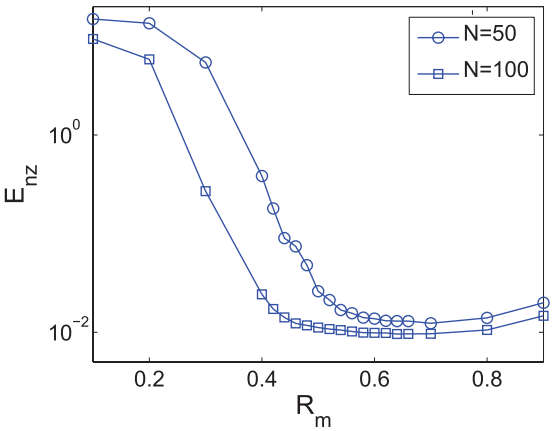

FIG. 7. (Color online) For uniform measurement noise, prediction error E_{nz} vs the normalized data amount R_m, where the networks are the same as in Fig. 6. The amplitude of additive noise is 5×10^{-5} for both curves. Each point is the result of averaging over 10 different network realizations.

We have also considered the issue of computational time. In our method, the main computational load lies in solving Eq. (11), which depends on the number of unknown coefficients and the number of measurements. We first fix the network sizes at $N = 100$ and record the computation time as the relative data amount R_m is changed. As shown in Fig. 8(a), the required time to reconstruct one coefficient vector (for one variable of one node in the network) scales approximately linearly with the data amount. Next we fix R_m and monitor the required computation time as a function of the network size. For linear coupling, the number of unknown coefficients is proportional to the network size N if it is sufficiently large. We set $R_m = 0.75$ to ensure accurate reconstruction in each case, so the amount of data used for reconstruction increases linearly with the number of unknown coefficients. Figure 8(b) shows the result, where the network size varies from $N = 20$ to $N = 500$. We see that the required computation time indeed increases approximately linearly with the number of unknown coefficients.

B. Prediction of network synchronizability from data

A full reconstruction of nodal dynamics allows us to calculate the MSF Ψ as a function of $K \equiv \xi\mu$ for any given coupling scheme. To be illustrative, we calculate the MSFs for four different coupling schemes ($x \to x$, $y \to x$, $z \to x$, and $z \to z$) for the coupled network of Lorenz oscillators, as shown in Fig. 9. These coupling patterns generate distinct behaviors of the MSF in terms of its number of zeros. If a region of $\Psi(K) < 0$ exists, emergence of stable synchronization is likely for the oscillator network, regardless of the network structure; otherwise synchronization is unlikely for any network structure. In Fig. 9, for example, for the $x \to x$ coupling scheme, there is a relatively large synchronization region for K beyond a critical value. For the $y \to x$ scheme, a synchronization region exists but its size is not as large as that for the case of $x \to x$ coupling. For the $z \to z$ coupling scheme, there are in fact two separated synchronization regions. In contrast, for the $z \to x$ coupling scheme, synchronization is unlikely because $\Psi(K)$ is positive

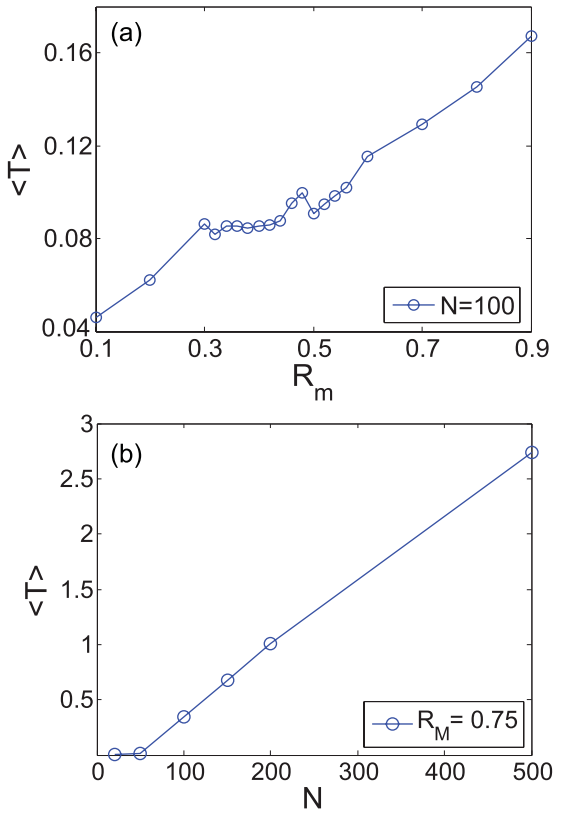

FIG. 8. (Color online) For weighted, random networks of Hénon maps, (a) the average computational time T (in arbitrary units) required for one variable on one node vs the data ratio R_m, for fixed network size ($N = 100$) and (b) T vs the network size N for fixed R_m (0.75) for which accurate reconstruction can be achieved. For both panels, 20 network realizations are used.

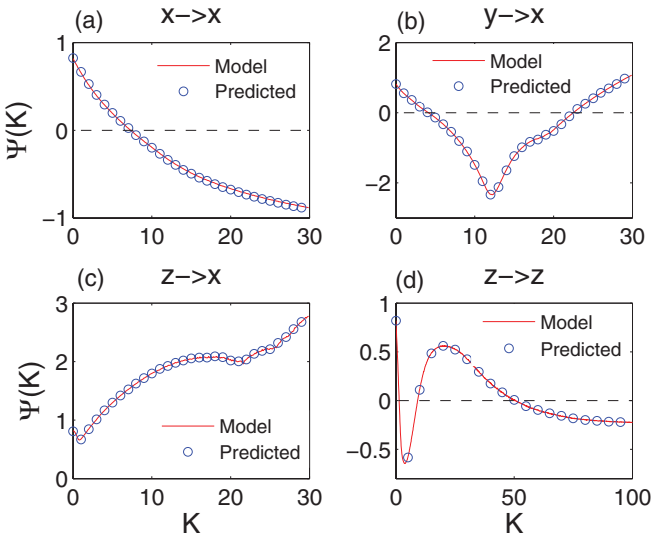

FIG. 9. (Color online) Comparison of MSFs calculated from predicted parameters (open circles) and from real ones (solid lines) for the random Lorenz oscillator network. Panels (a)–(d) are for coupling schemes $x \to x$, $y \to x$, $z \to x$, and $z \to z$, respectively. All time-series data are generated by the same oscillator network as in Fig. (2).

for all values of K. A more systematic analysis of the MSF behaviors for typical nonlinear oscillators can be found in Ref. [7]. The excellent agreement between the true and predicted MSFs shown in Fig. 9 suggests that our compressive-sensing-based approach can lead to a quite reliable estimate of the MSF at a quantitative level. Likewise, the boundaries between synchronous and asynchronous regions can also be precisely identified, rendering possible anticipation of the emergence of synchronization in the underlying network system.

To quantify the performance of our method in identifying the synchronization region, we define a measure of agreement, denoted by A_M, between the predicted and the true synchronization region, as exemplified in Fig. 9(b) for the $y \to x$ coupling scheme. Specifically, we denote the true synchronization region R_t by (K_a, K_b) in which the MSF is negative, and denote the predicted region R_p by (K'_a, K'_b). We thus define

$$A_M = \frac{R_p \bigcap R_t}{R_p \bigcup R_t} = \frac{\min(K_b, K'_b) - \max(K_a, K'_a)}{\max(K_b, K'_b) - \min(K_a, K'_a)}, \quad (16)$$

where generally $A_M \leqslant 1$. Two extreme cases are $A_M = 0$ when $R_p \bigcap R_t = \emptyset$ and $A_M = 1$ when $R_p = R_t$, which indicate perfect prediction. Results are shown in Fig. 10, where A_M approaches unity as the amount of measurement exceeds only about 65% of the number of assumed coefficients to be predicted. For the case of a single intersection K_a of a MSF with $\Psi(K) = 0$, as shown in Fig. 9(a) for the $x \to x$ coupling scheme, we can define an agreement measure in a similar way:

$$A_M = \frac{\min(K_a, K'_a)}{\max(K_a, K'_a)}, \quad (17)$$

where $0 \leqslant A_M \leqslant 1$. In cases where there are multiple synchronization regions, e.g., as happened for the $z \to z$ coupling scheme in Fig. 9(d), the agreement measure can be taken as the average of all measures, one calculated from each separate region.

IV. DATA-BASED ANTICIPATION AND CONTROL OF NETWORK SYNCHRONIZATION

Based on the reconstructed network structure and dynamics, we now propose a strategy to anticipate and control collective dynamics of complex oscillator networks. The base of control is prediction of future behavior by decoding the presently available time series. If the natural dynamics in the future is undesirable, one can implement a certain control scheme to drive the system to avoid the undesirable state before it occurs. This, however, requires relatively complete knowledge about the networked dynamical system, which, as we have demonstrated in Sec. III, can be achieved by exploiting the compressive-sensing paradigm.

To be concrete, we discuss the case where synchronization is a desirable state of operation for the system, under the assumption that the system is not synchronized at the present. The first step is to determine, from currently available time series, whether synchronization is intrinsically likely to emerge. An answer can be obtained by using the reconstructed network structure and dynamics to estimate the network eigenvalue spectrum and MSF. The answer can be affirmative, for example, if the MSF is predicted to be negative in an open generalized coupling-parameter interval. That the system is not currently synchronized indicates that the normalized eigenvalue spectrum does not fall into the interval and, hence, suitable control can be applied to rescale and shift the eigenvalue spectrum into the negative MSF interval. To illustrate this method, we use the network system of coupled chaotic Lorenz oscillators in Sec. III. Figure 11(a) shows some representative time series in a case where the network is not synchronized, and the corresponding MSF and eigenvalue spectrum calculated from the reconstructed network structure and dynamics are shown in Fig. 11(c). We see that for some values of K [data points in Fig. 11(c)], the products between the coupling strength ξ and eigenvalues μ are not located in the synchronizable region as indicated by the MSF

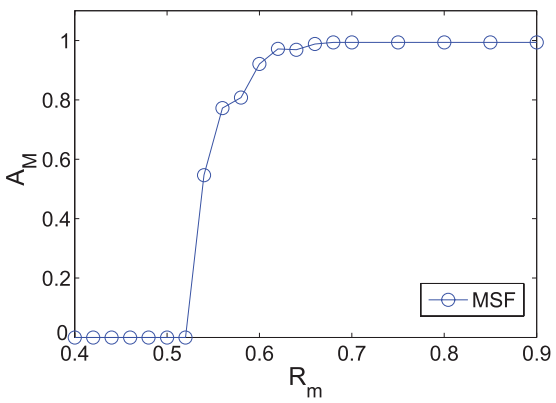

FIG. 10. (Color online) Measure of agreement of synchronization prediction, A_M, as a function of R_m for the MSF shown in Fig. 9(b), where the coupling scheme is $y \to x$.

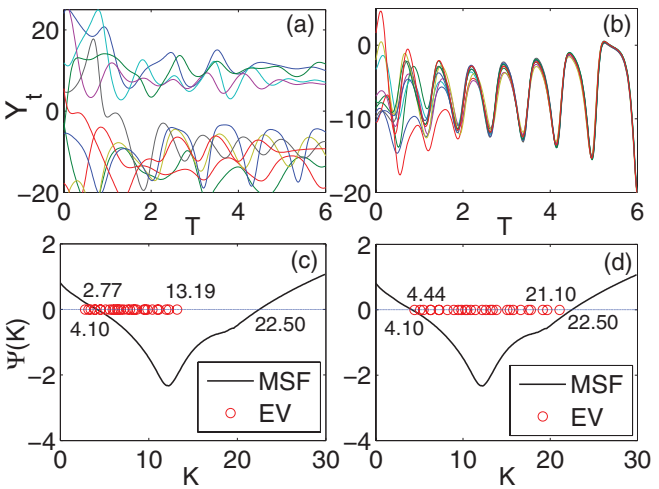

FIG. 11. (Color online) Time series of y component for 10 of the $N = 30$ nodes in two random networks of global coupling strength $\xi = 1$ and $\xi = 1.6$, respectively, for (a) a nonsynchronized network and (b) a synchronized network. Other parameters are the same for both bases: connection probability $p = 0.2$ and weight distribution interval of [0.9,1.0]. (c) and (d) Rescaled eigenvalues $K_i(=\xi\mu_i)$ (denoted by open circles) of the network coupling matrices with respect to the MSF (denoted by solid lines) inferred from the same nodal dynamics and coupling scheme from the time series in (a) and (b), respectively.

[curve in Fig. 11(c)]. Thus, at the current parameter setting, synchronization cannot be realized in the system. In order for synchronization to emerge, all K values must fall into a region where the MSF is negative. A simple and practical way to manipulate K is to adjust the coupling strength but to keep the nodal dynamics and network structure unchanged. When the coupling strength ξ is modified, the network system can indeed achieve synchronization, as shown by the synchronous time series in Fig. 11(b). Examination of the MSF and eigenvalue spectrum indicates that, indeed, in this case all K values fall into the negative MSF interval. We stress that a prerequisite to this simple control scheme is full knowledge of the network structure and dynamics, which, as we have demonstrated, can be faithfully reconstructed based solely on a small amount of data.

V. CONCLUSION AND DISCUSSION

Reconstructing dynamical systems based on time series is a problem of significant interest with broad applications in many areas of science and engineering. However, this problem has been outstanding in nonlinear dynamics because, despite previous efforts [34] in phase-space reconstruction using the standard delay-coordinate embedding method [35] to decode the topological properties of the underlying system, how to accurately infer the underlying *nonlinear system equations* remains largely an unsolved problem. In principle, a nonlinear system can be approximated by a large collection of linear equations in different regions of the phase space, which can indeed be achieved by reconstructing the Jacobian matrices on a proper grid that covers the phase-space region of interest [36, 37]. However, the accuracy and robustness of the procedure are challenging issues, involving the difficulty associated with the required computations. The recently emerged paradigm of compressive sensing [11–15] provides a possible approach to addressing the dynamical-system reconstruction problem [19,20]. In particular, our ability to fully reconstruct dynamical systems using only time-series data is based on the fact that the dynamics of natural and artificial systems are determined by smooth enough functions that can be approximated by finite expansions. The major task then becomes estimating the coefficients in the series representation of the vector field governing the system dynamics, for example, from a power-series expansion. In general, the power series can contain high-order terms, and the total number of coefficients to be estimated can therefore be quite large. This is a very difficult problem to solve, since large amounts of data would be needed, making the computations extremely demanding. However, most of these coefficients are either zero or negligible, rendering sparse the coefficient vector to be reconstructed, and enabling application of the compressive-sensing paradigm.

The main achievement of this paper is to extend our recently developed method of reconstructing dynamical systems [19,20] to complex *weighted* oscillator networks and then to address the problem of forecasting collective dynamics. In general, predicting the emergence of collective dynamics is an extremely difficult problem, and it is necessary to focus on a relatively well understood type of collective dynamics. We choose synchronization. We have detailed the basic principle of time-series-based prediction of synchronization in complex oscillator networks. We have also demonstrated, using a prototype of oscillator networks with nonuniform coupling strengths (so that the network is weighted), that our compressive-sensing approach can indeed fully reconstruct the network structure and dynamics, based on which the emergence of synchronous dynamics can be anticipated. We have also articulated and demonstrated a method, based on full reconstruction of a complex networked dynamical system that is not yet synchronized, to make it synchronizable by parameter adjustment.

One issue is the continuity of the available data. We wish to point out that compressive sensing in general does not depend strictly on this property of the observed time series. When constructing the linear equations, we need to approximate the derivatives of dynamical variables for all oscillators. Because of this, insofar as a small slice window of the time series (either continuous or discrete) is available so that the derivatives can be calculated, compressive sensing can be carried out to recover the network structures and nodal dynamics. In fact, slices of time series can be collected at different times to facilitate collection of measurements.

Another issue is the hidden dimensions, which presents a serious obstacle to network and dynamical-system reconstruction. This is similar to the case of searching for a power-expansion basis. If the expansion basis is not complete to cover all factors with significant magnitude, the error caused will be distributed onto the rest of the coefficients, leading to incorrect reconstruction. While this remains an outstanding problem in the reverse engineering of complex dynamical systems, we speculate that traditional nonlinear time-series analysis methods such as phase-space reconstruction may be used to determine the intrinsic dimension of the system prior to applying compressive sensing, which is an issue worth further investigation.

We emphasize that a full reconstruction of a complex oscillator networked system from time series is possible only when the system is not in synchronization, and the information can then be used to forecast or anticipate synchronization in the future. If the system is already synchronized, time series from different nodes are practically identical so that it is not possible to reconstruct the network structure. However, there may exist a solution to this problem. In particular, given a network system that is already synchronized, we hypothesize using small, random, and rare perturbations to disturb the system so that it desynchronizes temporally. Since the synchronization state is stable, the system will settle back to being synchronous quickly. However, the window of temporal desynchronization provides us with an opportunity to probe the system structure. While the transient desynchronization phase may be short, our compressive-sensing method can be particularly suitable because of the extremely low data requirement.

ACKNOWLEDGMENTS

We thank Dr. Liang Huang for extremely valuable and stimulating discussions. This work was supported by AFOSR under Grant No. FA9550-10-1-0083 and by NSF Grants No. CDI-1026710 and No. BECS-1023101. Wen-Xu Wang acknowledge NSFC under Grant No. 11105011.

[1] P. W. Anderson, Science **177**, 393 (1972).

[2] S. Strogatz, *Sync: The Emerging Science of Spontaneous Order* (Hyperion, New York, 2003).

[3] A. S. Pikovsky, M. G. Rosenblum, and J. Kurths, *Synchronization: A Universal Concept in Nonlinear Sciences* (Cambridge University Press, New York, 2003).

[4] L. M. Pecora and T. L. Carroll, Phys. Rev. Lett. **64**, 821 (1990).

[5] There is a large body of literature on network synchronization. See, for example, M. Barahona and L. M. Pecora, Phys. Rev. Lett. **89**, 054101 (2002); X. F. Wang and G. Chen, Int. J. Bifurcation Chaos Appl. Sci. Eng. **12**, 187 (2002); IEEE Trans. Circuit Syst. I **49**, 54 (2002); T. Nishikawa, A. E. Motter, Y.-C. Lai, and F. C. Hoppensteadt, Phys. Rev. Lett. **91**, 014101 (2003); M. Chavez, D.-U. Hwang, A. Amann, H. G. E. Hentschel, and S. Boccaletti, *ibid*. **94**, 218701 (2005); L. Huang, K. Park, Y.-C. Lai, L. Yang, and K. Yang, *ibid*. **97**, 164101 (2006); V. Belykh, I. Belykh, and M. Hasler, Physica D **224**, 42 (2006).

[6] L. M. Pecora and T. L. Carroll, Phys. Rev. Lett. **80**, 2109 (1998).

[7] L. Huang, Q.-F. Chen, Y.-C. Lai, and L. M. Pecora, Phys. Rev. E **80**, 036204 (2009).

[8] M. K. S. Yeung, J. Tegnér, and J. J. Collins, Proc. Natl. Acad. Sci. USA **99**, 6163 (2002).

[9] D. di Bernardo, M. J. Thompson, T. S. Gardner, S. E. Chobot, E. L. Eastwood, A. P. Wojtovich, S. J. Elliott, S. E. Schaus, and J. J. Collins, Nat. Biotechnol. **23**, 377 (2005).

[10] S. Gorur Shandilya, and M. Timme, New J. Phys. **13**, 013004 (2011).

[11] E. Candes, J. Romberg, and T. Tao, IEEE Trans. Inf. Theory **52**, 489 (2006); Commun. Pure Appl. Math. **59**, 1207 (2006).

[12] E. Candes, in *Proceedings of the International Congress of Mathematicians, Madrid, Spain* (European Mathematical Society, Zürich, Switzerland, 2006).

[13] D. Donoho, IEEE Trans. Inf. Theory **52**, 1289 (2006).

[14] R. G. Baraniuk, IEEE Signal Process. Mag. **24**, 118 (2007).

[15] E. Candes and M. Wakin, IEEE Signal Process. Mag. **25**, 21 (2008).

[16] P. Erdös and A. Rényi, Publ. Math. Debrecen, **6**, 290 (1959).

[17] E. N. Lorenz, J. Atmos. Sci. **20**, 130 (1963).

[18] M. Hénon, Commun. Math. Phys. **50**, 69 (1976).

[19] W.-X. Wang, R. Yang, Y.-C. Lai, V. Kovanis, and C. Grebogi, Phys. Rev. Lett. **106**, 154101 (2011).

[20] W.-X. Wang, R. Yang, Y.-C. Lai, V. Kovanis, and M. A. F. Harrison, Europhys. Lett. **94**, 48006 (2011).

[21] S. Fortunato, Phys. Rep. **486**, 75 (2010).

[22] T. S. Gardner, D. di Bernardo, D. Lorenz, and J. J. Collins, Science **301**, 102 (2003).

[23] S. Grün, M. Diesmann, and A. Aertsen, Neural Comput. **14**, 43 (2002).

[24] R. Gütig, A. Aertsen, and S. Rotter, Neural Comput. **14**, 121 (2002).

[25] G. Pipa and S. Grün, Neurocomputing **52**, 31 (2003).

[26] J. Bongard and H. Lipson, Proc. Natl. Acad. Sci. USA **104**, 9943 (2007).

[27] M. Timme, Phys. Rev. Lett. **98**, 224101 (2007).

[28] D. Napoletani and T. D. Sauer, Phys. Rev. E **77**, 026103 (2008).

[29] W.-X. Wang, Q. Chen, L. Huang, Y.-C. Lai, and M. A. F. Harrison, Phys. Rev. E **80**, 016116 (2009).

[30] J. Ren, W.-X. Wang, B. Li, and Y.-C. Lai, Phys. Rev. Lett. **104**, 058701 (2010).

[31] Z. Levnajić and A. Pikovsky, Phys. Rev. Lett. **107**, 034101 (2011).

[32] S. Hempel, A. Koseska, J. Kurths, and Z. Nikoloski, Phys. Rev. Lett. **107**, 054101 (2011).

[33] Similar construction methods of such linear equations have been proposed in Refs. [8] and [10].

[34] H. Kantz and T. Schreiber, *Nonlinear Time Series Analysis* (Cambridge University Press, Cambridge, UK, 1997).

[35] F. Takens, in *Dynamical Systems and Turbulence*, edited by D. A. Rand and L.-S. Young, Lecture Notes in Mathematics, Vol. 898 (Springer-Verlag, New York, 1981).

[36] J. D. Farmer and J. J. Sidorowich, Phys. Rev. Lett. **59**, 845 (1987).

[37] T. D. Sauer, Phys. Rev. Lett. **93**, 198701 (2004).